Large-eddy-simulation of 3-dimensional Rayleigh-Taylor instability in incompressible fluids

WANG Lili (王丽丽)[1,2], LI Jiachun (李家春)[1] & XIE Zhengtong (谢正桐)[1]

1. Institute of Applied Physics and Computational Mathematics, Beijing 100088, China;
2. LNM, Institute of Mechanics, Chinese Academy of Science, Beijing 100080, China;
3. DES, Institute of Mechanics, Chinese Academy of Sciences, Beijing 100080, China

Received June 15, 2001

Abstract The 3-dimensional incompressible Rayleigh-Taylor instability is numerically studied through the large-eddy-simulation (LES) approach based on the passive scalar transport model. Both the instantaneous velocity and the passive scalar fields excited by sinusoidal perturbation and random perturbation are simulated. A full treatment of the whole evolution process of the instability is addressed. To verify the reliability of the LES code, the averaged turbulent energy as well as the flux of passive scalar are calculated at both the resolved scale and the subgrid scale. Our results show good agreement with the experimental and other numerical work. The LES method has proved to be an effective approach to the Rayleigh-Taylor instability.

Keywords: **Rayleigh-Taylor instability, large-eddy-simulation, passive scalar, turbulent mixing.**

The Rayleigh-Taylor instability of an interface between two fields with different densities occurs when the density gradient is opposite to the gravitational field. It appears in both technological applications and natural phenomena, such as inertial confinement fusion (ICF), supernova dynamics, high speed collision, phase change and combustion.

The growth of Rayleigh-Taylor instability can be roughly divided into four stages[1]. During the first stage the amplitude of the perturbation is much smaller than the wavelength λ. The linear theory is valid and the interface exhibits exponential growth

$$h(t) = h_0 e^{\alpha t},$$

where $h(t)$ is the amplitude at time t, h_0 is the initial amplitude, and α is the growth rate of the perturbation dependent on the density ratio, viscosity, surface tension, etc. The instability evolves into the nonlinear stage when the amplitude exceeds $0.1—0.4\lambda$. At this stage the moving interface becomes rising bubbles on the side of the heavy fluid and falling spikes on the side of the heavy fluid. Next, the non-linearity becomes much stronger and the Kelvin-Helmholtz instability occurs due to the difference between the tangential velocities of the two fluids at the interface. In this way the spike rolls up at the tail and the mushroom comes into being. Besides, more complicated behavior appears in consideration of random perturbation, which includes competition and merging between bubbles with different scales. At the last stage, the contour profiles of the two fluids penetrate each other and the turbulent mixing regime is achieved finally.

The Rayleigh-Taylor instability is a complicated phenomenon containing nonlinearity, discontinuity, non-stability, multi-scale effect and so on. Up to now the law of the whole process is poorly understood. The analytic and quasi-analytic methods can only deal with the first two stages. The behavior during the later stages is mainly studied through numerical or experimental

approaches. With tremendous progress in scientific computing, the numerical simulation of Rayleigh-Taylor instability is undergoing a blooming development during the past two decades. Various schemes have been performed by a number of scholars, such as the vortex method[2,3], the level set method[4—6], the front tracking scheme[7], the lattice Boltzmann scheme[8], etc. These simulations have revealed several interesting properties, such as the evolution of bubbles and spikes, during the nonlinear stage and the thickness of the mixing layer versus time with random perturbation. But a full treatment of the interfacial motion is still beyond the capability of existing numerical studies. Little is known about the turbulent mixing stage. This is mainly due to the following facts: First of all, there is a discontinuity across the interface. Thus the governing equations are singular exactly at the interface, either in their coefficients or their source terms or both. The second is the difficulty in tracking the fracted interface in calculation. And the most important one is that the flow involves turbulent mixing. The small length scale effect is inaccessible to feasible calculations. Except for the lattice Boltzmann scheme, all the methods encounter difficulties in dealing with the final stage.

In this paper the large-eddy-simulation(LES) scheme, together with the passive scalar transport model, is adopted to solve these knottiness. Evolution of the interface and the mixing process are investigated through the concentration field of the passive scalar without tracking the interface. The small length scale effect is calculated by using the turbulence energy model in LES. With inclusion of the molecular diffusion in momentum and energy, the LES code presented here is adaptive to the full evolution of the instability.

1 Physical model and the large-eddy-simulation scheme

1.1 Boussinesq hypothesis and the governing equations for LES

Consider two homogeneous fluids with different densities in a stationary accelerated field. The Rayleigh-Taylor instability occurs when the heavy fluid is located upon the light one in gravity field. The fluids we studied are boundless in the horizontal direction with fixed top and bottom walls. The motion can be described with a passive scalar transport model in which a single-phase fluid dissolving diluted passive scalar is used. The convection and diffusion of the passive scalar result in the redistribution in density. The Boussinesq hypothesis is adopted here when the density ratio approaches 1. In other words, the fluid is assumed to be incompressible and only the variation in density is taken into account.

The direct numerical simulation (DNS) is difficult to implement here because the turbulent mixing stage contains motions with a broad range of scales. In this paper the large-eddy-simulation (LES) is used, in which the small length scale effect is simulated through the subgrid scale stress and flux. With LES, the large eddies are simulated explicitly, while the small eddies are parmeterized. So the CPU time and storage demands are greatly reduced in LES as compared with those in DNS. Meanwhile, the instantaneous field can be achieved with a wide range. It is especially suitable to deal with the problem of boundless Rayleigh-Taylor instability.

The variables for the resolved scale, $\bar{F}(\boldsymbol{x}, t)$, is defined by using the Leonard's filter as follows:

$$\bar{F} = (x, t) = \int_D G(x - x') F(x', t) \mathrm{d}x', \tag{1}$$

where the integration is over the whole flow domain D. The filtering function $G(\cdot)$ is taken as the Gaussian function in the horizontal directions

$$G(x - x') = \left(\sqrt{\frac{\gamma/\pi}{\Delta}}\right)^2 \exp[-(\sqrt{\gamma/\Delta})^2(x - x')^2], \tag{2}$$

whereas the top-hat function is applied in the vertical direction

$$G = \frac{1}{\Delta^3}, \tag{3}$$

where γ is a constant, and Δ the filter width.

Applying the filtering operator to the continuity equation and the incompressible Navier-Stokes equations, we have the following governing equations for the resolved scale components:

$$\frac{\partial \bar{u}}{\partial x} + \frac{\partial \bar{v}}{\partial y} + \frac{\partial \bar{w}}{\partial z} = 0, \tag{4}$$

$$\frac{\partial \bar{u}}{\partial t} = \overline{\bar{v}\zeta_z} - \overline{\bar{w}\zeta_y} - \frac{\partial P^*}{\partial x} - \frac{\partial \langle \bar{p} \rangle}{\partial x} + \frac{\partial \tau_{xx}}{\partial x} + \frac{\partial \tau_{xy}}{\partial y} + \frac{\partial \tau_{xz}}{\partial z}, \tag{5}$$

$$\frac{\partial \bar{v}}{\partial t} = \overline{\bar{w}\zeta_x} - \overline{\bar{u}\zeta_z} - \frac{\partial P^*}{\partial y} - \frac{\partial \langle \bar{p} \rangle}{\partial y} + \frac{\partial \tau_{xy}}{\partial x} + \frac{\partial \tau_{yy}}{\partial y} + \frac{\partial \tau_{yz}}{\partial z}, \tag{6}$$

$$\frac{\partial \bar{w}}{\partial t} = \overline{\bar{u}\zeta_y} - \overline{\bar{v}\zeta_x} - \frac{a\bar{\rho}}{\rho_0} - \frac{\partial P^*}{\partial z} + \frac{\partial \tau_{xz}}{\partial x} + \frac{\partial \tau_{yz}}{\partial y} + \frac{\partial \tau_{zz}}{\partial z} - \left\langle \overline{\bar{u}\zeta_y} - \overline{\bar{v}\zeta_x} - \frac{a\bar{\rho}}{\rho_0} - \frac{\partial P^*}{\partial z} + \frac{\partial \tau_{xz}}{\partial x} + \frac{\partial \tau_{yz}}{\partial y} + \frac{\partial \tau_{zz}}{\partial z} \right\rangle, \tag{7}$$

where the overbar denotes the resolved scale field, the angular brackets denote horizontal means, a is the acceleration, ρ the density, ρ_0 the mean density of the two fluids, ζ_i the vorticity component, and τ_{ij} the subgrid scale Reynolds stresses are defined as

$$\tau_{ij} = R_{ij} - R_{kk}\delta_{ij}/3, \tag{8}$$

$$R_{ij} = \overline{u'_i u'_j} + \overline{u'_i \bar{u}_j} + \overline{\bar{u}_i u'_j}, \tag{9}$$

$$P^* = \frac{\bar{p}}{\rho_0} + \frac{R_{kk}}{3} + \frac{(\overline{\bar{u}_k \bar{u}_k})}{2}. \tag{10}$$

and the passive scalar transportation equation

$$\frac{\partial \bar{\theta}}{\partial t} = -\overline{\bar{u}\frac{\partial \bar{\theta}}{\partial x}} - \overline{\bar{v}\frac{\partial \bar{\theta}}{\partial y}} - \overline{\bar{w}\frac{\partial \bar{\theta}}{\partial z}} + \frac{\partial \tau_{\theta x}}{\partial x} + \frac{\partial \tau_{\theta y}}{\partial y} + \frac{\partial \tau_{\theta z}}{\partial z}. \tag{11}$$

θ is the passive scalar, that is, the density ρ here, and $\tau_{\theta i}$ the subgrid turbulence fluxes of virtual passive scalar.

The turbulence energy model used by Deardorff[14] is adopted, and a prognostic equation is solved for the SGS kinetic energy as follows:

$$\frac{\partial \overline{e'}}{\partial t} = -\overline{\bar{u}_i \frac{\partial \overline{e'}}{\partial x_i}} - \overline{u'_i u'_j}\frac{\partial \bar{u}_i}{\partial x_j} + \frac{a}{\theta_0}\overline{w'\theta''} - \frac{\partial \overline{[u'_i(e' + p'/\rho_0)]}}{\partial x_i} - \varepsilon, \tag{12}$$

where ε is the dissipation rate.

1.2 Subgrid scale (SGS) model

The turbulence energy model is usually adopted to deal with the buoyancy-driven flow in LES, in which the eddy viscosity coefficient is directly supposed to be proportional to the SGS velocity scale ($\overline{e'}^{1/2}$) and a certain characteristic length l. With the molecular diffusion included in momentum and energy, the SGS fluxes can be expressed in terms of the resolved scale field as

$$\tau_{ij} = (K_M + \nu)\left(\frac{\partial \bar{u}_i}{\partial x_j} + \frac{\partial \bar{u}_j}{\partial x_i}\right), \tag{13}$$

$$\tau_{\theta i} = (K_H + k)\frac{\partial \bar{\theta}}{\partial x_i}, \tag{14}$$

where K_M, K_H are the SGS eddy coefficients for momentum and passive scalar; v and k are the molecular diffusivities for momentum and mass diffusion correspondingly.

The closure assumptions made here to solve (12) are the down-gradient diffusion assumption

$$\overline{u'_i(e' + p'/\rho_0)} = -2K_M\frac{\partial \overline{e'}}{\partial x_i}, \tag{15}$$

and the Kolmogoroff hypothesis

$$\varepsilon = \frac{C\overline{e'}^{3/2}}{l}, \tag{16}$$

with

$$C = 0.19 + \left(0.51\frac{l}{\Delta S}\right), \tag{17}$$

$$\Delta S = (\Delta x \Delta y \Delta z)^{1/3}. \tag{18}$$

According to the SGS model suggested by Deardorff[14] and Moeng[18], the eddy diffusivity coefficients are expressed as

$$K_M = 0.1 l \overline{e'}^{1/2}, \tag{19}$$

$$K_H = \left[1 + 2\frac{l}{\Delta S}\right]K_M, \tag{20}$$

while the length scale l is given by

$$l = \min\left\{\Delta S,\ 0.76\overline{e'}\left(\frac{g}{\theta_0}\frac{\partial \bar{\theta}}{\partial z}\right)^{-\frac{1}{2}}\right\}. \tag{21}$$

1.3 Numerical scheme

The periodic boundary conditions are applied in both x and y directions, while the non-slip boundary condition is applied in z direction. The simulation is carried out on $32 \times 32 \times 128$ grids. Initially each of the two fluids occupies half of the computational domain.

A mixed scheme of Fourier expansion in the horizontal directions and finite difference in the vertical direction are therefore appropriate for the simulation. The pseudo-spectral method is chosen to evaluate the horizontal derivatives. To calculate the x-derivatives of $\bar{u}$, for example, the variable $\bar{u}$ is firstly transformed into the Fourier space in x:

$$\hat{\bar{u}}(k_m, y, z) = \frac{1}{N}\sum_{n=1}^{N}\bar{u}(x_n, y, z)\exp(-ik_m x_n). \tag{22}$$

Then the transform coefficient $\hat{\bar{u}}$ is multiplied by ik_m, and $ik_m\hat{\bar{u}}$ is inversely transformed back into the grid points using

$$\left(\frac{\partial \bar{u}}{\partial x}\right)_n = \sum_{m=-(N/2)+1}^{N/2} ik_m \hat{\bar{u}}(k_m, y, z)\exp(ik_m, x_n), \tag{23}$$

where N is the number of grid points in this direction, and $k_m = \dfrac{2\pi m}{N\Delta x}$ is the wave-number.

The centered finite-differences of second-order accuracy are used to evaluate the vertical derivatives. And the time advancement is integrated using the Adams-Bathoforth scheme. $\bar{w}$ is located at the up-and-down layers of the grid, while $\bar{u}$, $\bar{v}$, $\bar{\theta}$, $\bar{p}$, $\overline{e'}$ are located at the center of the grid.

2 Validation of the code

The Rayleigh-Taylor instability experiences laminar, transitional and turbulent flow stages. To make the LES code adaptable to the full process of the interfacial motion, two terms are contained in the SGS fluxes in this paper (see eqs. (13) and (14)). $v\left(\frac{\partial \bar{u}_i}{\partial x_j}+\frac{\partial \bar{u}_j}{\partial x_i}\right)$, and $k\frac{\partial \bar{\theta}}{\partial x_i}$ are introduced to calculate the effect of the molecular diffusion, while K_M and K_H are due to the turbulent mixing. At the beginning, the SGS turbulent energy is quite weak. Because $K_M\left(\frac{\partial \bar{u}_i}{\partial x_j}+\frac{\partial \bar{u}_j}{\partial x_i}\right)$ and $K_H\frac{\partial \bar{\theta}}{\partial x_i}$ are proportional to the SGS velocity scale, we have

$$K_M \ll v, \qquad K_H \ll k$$

(fig. 1). That is to say, K_M and K_H can be neglected. In this case the LES is in fact a DNS. Because the motion is a laminar flow during this period, the grid is fine enough to solve all scales present in the flow.

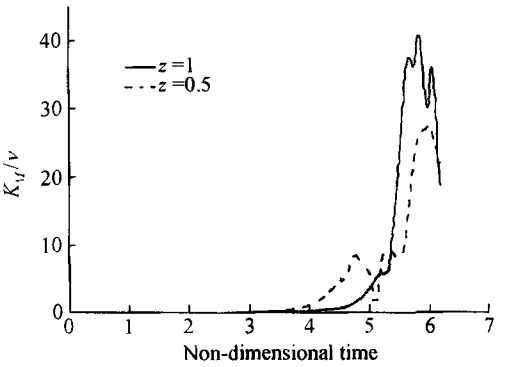

Fig. 1

On the contrary, the turbulent dissipation is much stronger at later stages when

$$K_M \gg v,$$
$$K_H \gg k.$$

Then T_M and K_H are dominant in (13) and (14). At this time, the small length scale effect is simulated through $K_M\left(\frac{\partial \bar{u}_i}{\partial x_j}+\frac{\partial \bar{u}_j}{\partial x_i}\right)$ and $K_H\frac{\partial \bar{\theta}}{\partial x_i}$. So we say that the mathematical model and programming code proposed here can deal with the whole process of Rayleigh-Taylor instability. In the next section we will show that the numerical results are in good agreement with other work.

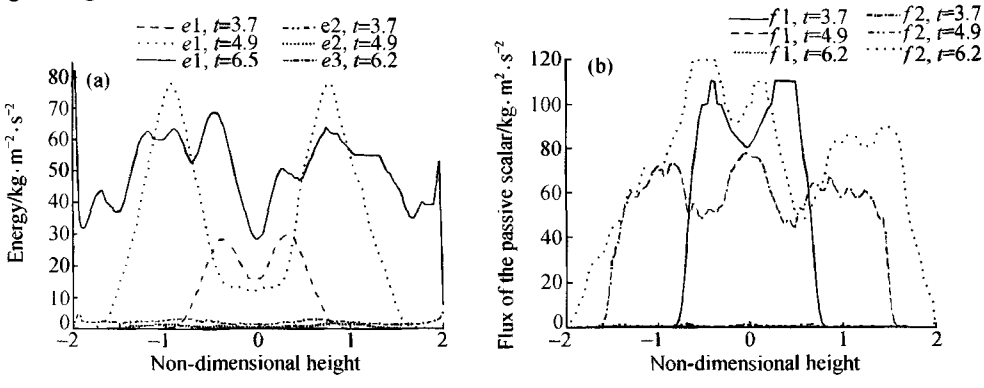

Fig. 2

The kinetic energy and flux of passive scalar of both the resolved scale and the subgrid scale are simulated for further validation. As shown in fig. 2(a), (b), the small eddies contribute much less passive scalar and momentum transport than the large eddies, and the energy contained within them is much weaker.

To verify the grid convergence of the code, the simulation is also carried out on 64 × 64 × 192 grids. As shown in fig. 3, the roll-up due to the Kelvin-Helmholtz instability is more pronounced on refined grids, whereas the structure in large scale and the macroscopic character of the flow remain the same. So we can say that the code used here is basically convergent within the range we discussed.

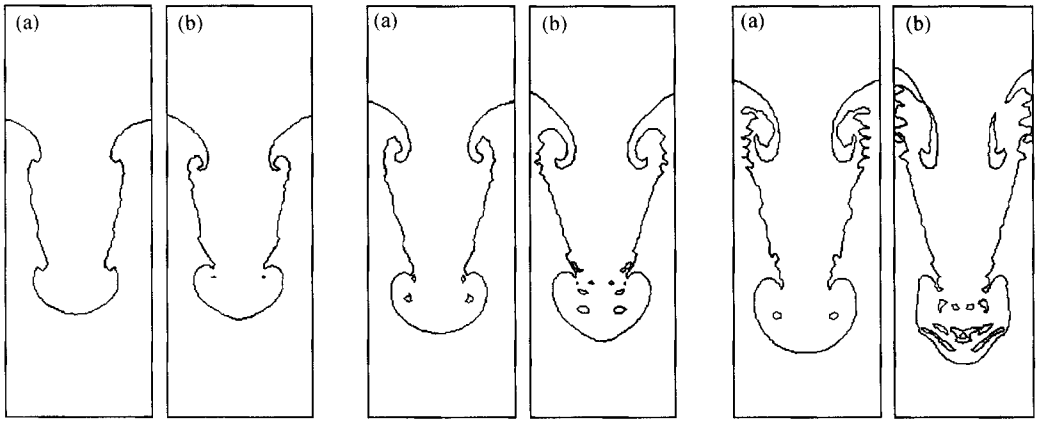

Fig. 3

3 Numerical results

Several factors, such as density ratio, acceleration, initial perturbation, compressibility, surface tension and viscosity, may affect the behavior of Rayleigh-Taylor instability. With surface tension and compressibility neglected, we only consider the viscosity in this paper. The control parameters we discussed here are the Atwood number $\left(A = \frac{\rho_u - \rho_l}{\rho_u + \rho_l} \right)$ and the acceleration.

Let us look at the motion from 2-dimensional (2D) and 3-dimensional (3D) sinusoidal perturbations first. The initial velocity fields are given by

2D pertubration:

$$u_0 = B\sin kx \cdot e^{-\alpha|z|} \cdot \mathrm{sign}(z),$$
$$v_0 = 0,$$
$$w_0 = \frac{Bk}{\alpha}\cos kx \cdot e^{-\alpha|z|};$$

and 3D perturbation:

$$u_0 = B\sin kx \cdot e^{-\alpha|z|} \cdot \mathrm{sign}(z),$$
$$v_0 = B\sin ky \cdot e^{-\alpha|z|} \cdot \mathrm{sign}(z),$$
$$w_0 = \frac{Bk}{\alpha}(\cos kx + \cos ky)e^{-\alpha|z|},$$

which satisfy the continuity equation.

The diffusion processes of the passive scalar from 2D and 3D perturbation are illustrated in figs. 4 and 5, respectively. Fig. 4 is the gray-scale view of the concentration field in 2D perturbation case, at the cross-section $x - z$, while fig. 5 is that of 3D at $x = y$. The Atwood number

is 0.1, and the acceleration equals 10 times the gravitational one.

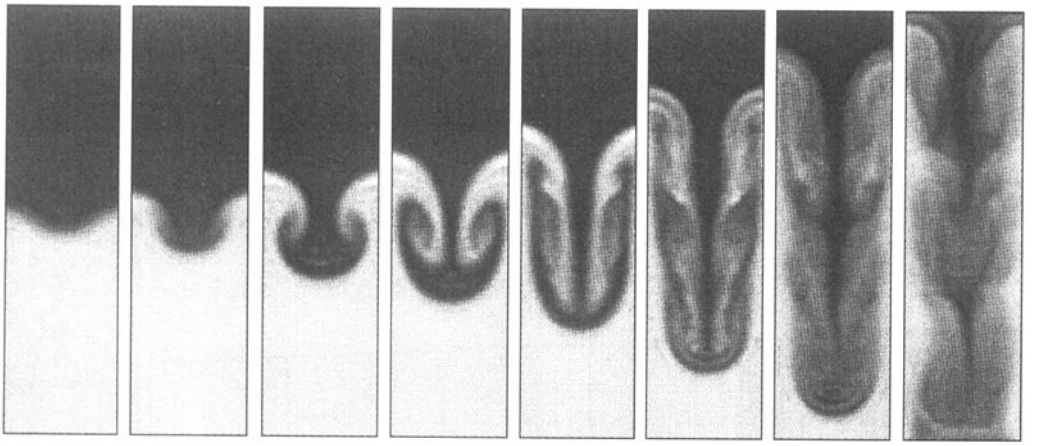

T=2.5 T=3.3 T=4.1 T=4.9 T=5.7 T=6.5 T=7.3 T=8.1

Fig. 4

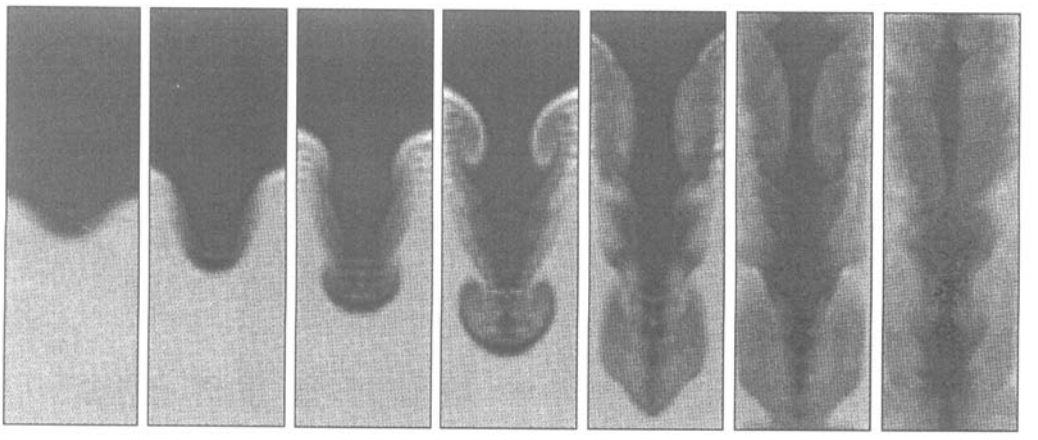

T=2.5 T=3.3 T=4.1 T=4.9 T=5.7 T=6.5 T=7.3

Fig. 5

With the surface tension neglected, the interface of the two fluids can be described by the contour of the passive scalar at level $\frac{\rho_u + \rho_l}{2}$. Evolution of the interface is shown in figs. 6 and 7. For both cases there are complex phenomena, including the linear growth of the interface, formation of spikes and bubbles, roll-up on the side of the spikes, penetration between the two fluids, and chaotic mixing. Take the motion from 3D perturtation in fig. 7 as an example. When $t < 2.5$, the amplitude of the perturbation is much smaller than the wavelength. The interface maintains the sinusoidal shape and the flow field is symmetrical up-and-down. At $t = 3.3$, the nonlinear growth starts. The interface develops into bubbles on the side of heavy fluid and spikes on the side of light fluid. At $t = 4.1$, the spike rolls up and mushroom comes into being due to

the Kelvin-Helmholtz instability. Besides, different from the 2D case, a two-layer roll-up phenomenon can be observed in the 3D circumstance. At $t = 4.9$—5.7, the shape of the interface becomes more complicated with lots of detailed structures. After that the interface breaks down and results in turbulent mixing. A similar evolution may be observed in other numerical simulations[6,9,10] although they were not carried out to this late stage.

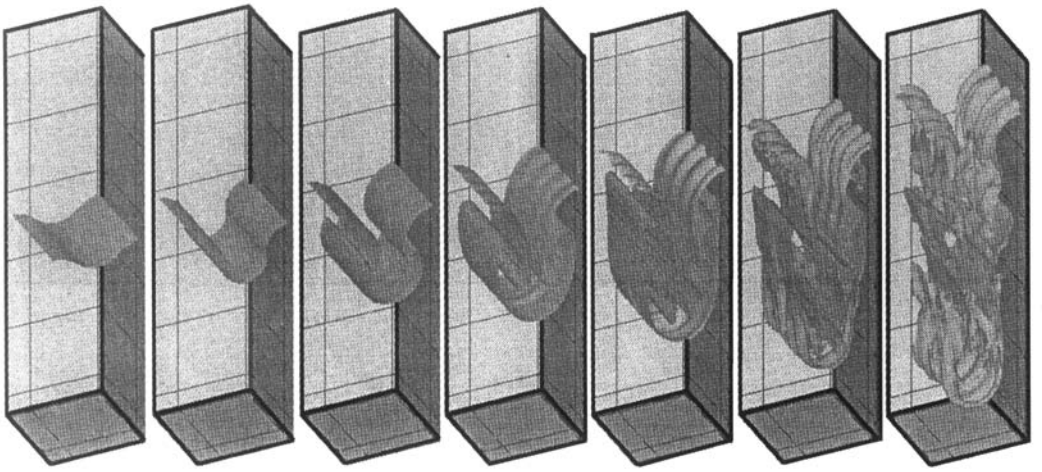

T=2.5 T=3.3 T=4.1 T=4.9 T=5.7 T=6.5 T=7.3

Fig. 6

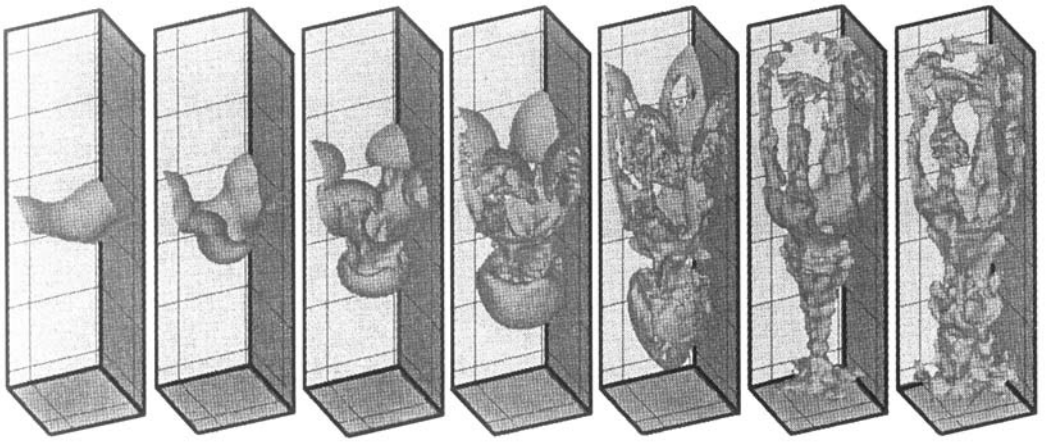

T=2.5 T=3 3 T=4.1 T=4.9 T=5.7 T=6.5 T=7.3

Fig. 7

There are some remarkable differences betweent the two cases:

1) The evolution of the instability is faster in the case with 3D perturbation.

2) The effect due to the Kelvin-Helmholz instability is more pronounced in the 2D case.

3) In the 3D case a two-layer roll-up phenomenon can be observed. The same trends were reported in other papers[9,10]. It was called the saddle point in ref. [9] where the new roll-up e-

merges. Also the interface is more complex with a lot of structures in small scale during the late stage in this case.

The features of Rayleigh-Taylor instability can be better illustrated via the velocity field shown in fig. 8. At the initial stage, there are two symmetrical vortices at the location of the primordial interface. With the elapse of time, the vortices are stretched and distorted. At $t = 4.1$, a single vortex is split into two vortices. Meanwhile, another vortex with smaller scale is generated between them. At $t = 6.5$, all the vortices are highly distorted. More and more detailed structures with smaller scales emerge until a regime of turbulent mixing have been achieved.

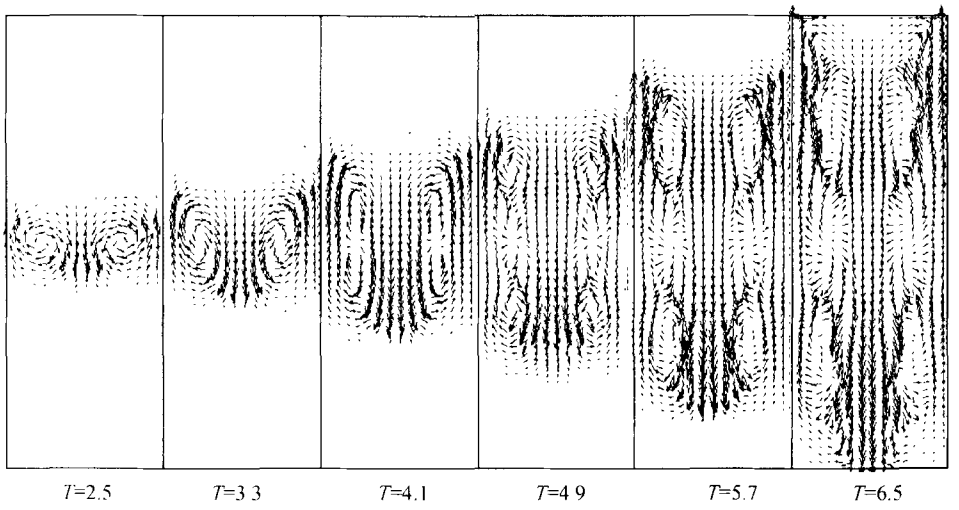

Fig. 8

The rule of Rayleigh-Taylor instability is still poorly understood now. The velocities of bubble and spike are the most commonly discussed ones within the few quantitative characteristic parameters in this problem. Fig. 9 shows the evolutions of the bubble and spike front in the 3D perturbation case. The growth of the bubble and spike is consistent with the theoretically predicted exponential growth in the early stage. At the nonlinear stage the bubble tends to grow at a constant speed. The terminal velocity of the bubble is expressed in the following form by Taylor:[11]

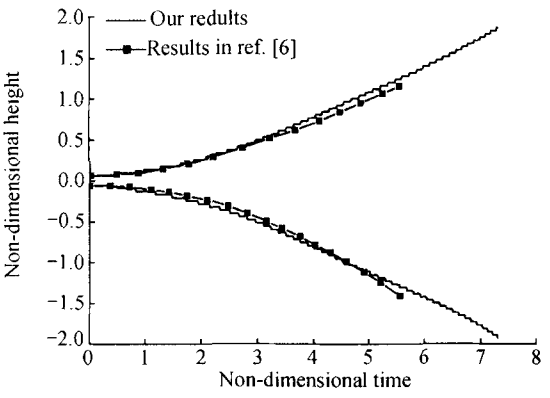

Fig. 9

$$v_b = C\sqrt{g\lambda/2}, \tag{24}$$

where C is a constant. For the 3D sinusoidal perturbation, Taylor's experimental result show that $C \approx 0.49$ when the Atwood number approaches 1. Numerical results of several schemes[6,8,9,12] with different Atwood numbers vary in the range 0.32—0.63. Our results are within 0.31—0.39. In table 1, the results of several simulations are presented.

Table 1

A	1 (Taylor)	0.82 (ref.[10])	0.67 (ref.[10])	0.33 (ref.[10])	0.5 ((ref.[9]))	0.33 (this paper)	0.2 (this paper)	0.1 (this paper)
C	0.49	0.50	0.46	0.36	0.43	0.39	0.32	0.31
$C/\sqrt{A}$	0.49	0.55	0.56	0.63	0.61	0.67	0.71	0.98

For Atwood number $A = 0.33$, the value of C obtained in this paper is close to that reported in ref.[6]. Based on the Boussinesq hypothesis, the approach presented here is not suitable to the case with large density ratio. Our numerical results with small Atwood number shows that C decreases as the Atwood number decreases. And $C/\sqrt{A}$ is not a constant as predicted in ref. [13] but is a variable which increases when the Atwood number decreases. The same trend is reported by Li[6] for compressible fluid.

In real situations the instability may possibly grow from a random perturbation. Up to now the behavior of this motion is far from being understood. The thickness of the mixing layer is usually used to describe the nature of the mixing. Both experiment of Read[15] and numerical results of Youngs[16,17] show that the thickness increases approximately quadratically with time, which can be expressed as

$$h_{AV}(t) = \alpha A g t^2, \tag{25}$$

where n_{AV} is the distance between the bubble front and the initial position of the interface. For the incompressible fluid, Read and Youngs concluded that α is almost a constant with different fluids and different values of acceleration. Using the level set method, Li[6] found that α is dependent on the compressiblity for comporessible fluid.

The thickness of the mixing layer, H, discussed in this paper is defined by letting the horizontal mean densities at the upper layer ($\bar{\rho}^+$) and lower layer ($\bar{\rho}^-$) be

$$\bar{\rho}^+ = \rho_u - 0.01(\rho_u - \rho_l),$$
$$\bar{\rho}^- = \rho_u - 0.99(\rho_u - \rho_l).$$

Let the initial velocity field be in the following form:

$$u_0 = \sum_{k=1}^{N} B_k \cos kx \cdot \sin ky \cdot e^{-\alpha|z|} \cdot \mathrm{sign}(z),$$
$$v_0 = \sum_{k=1}^{N} B_k \sin kx \cdot \cos ky \cdot e^{-\alpha|z|} \cdot \mathrm{sign}(z),$$
$$w_0 = -\sum_{k=1}^{N} \frac{B_k}{\alpha} \sin kx \cdot \sin ky \cdot e^{-\alpha|z|},$$

where B_k is random, and $N = 4$.

The interface at two moments is plotted in fig. 10. The scale of the interfacial structure is enlarged with time because the large bubbles will take over the adjacent smaller ones during the evolution. The thickness of the mixing layer versus time is shown in fig. 11, with the Atwood number of 0.1. By curve fitting we have

$$H(t) = 0.165 A g t^2. \tag{26}$$

Comparing eq. (26) with eq. (25), we have $\alpha \approx 0.08$. The results obtained in ref.[6] for fluids with two different compressibilities are $\alpha \approx 0.07$ and $\alpha \approx 0.06$.

4 Conclusions

A passive scalar transport model together with the LES scheme is proposed to study the 3D

Rayleigh-Taylor instability. The coherent structure in large length scale, and most quantities of energy and momentum are captured. The characteristic behavior and the principle of the interfacial motion from both sinusoidal and random perturbations are achieved. Several cases are dealt with to verify the reliability of the LES code. The numerical results show good qualitative agreement with experiments and other numerical studies.

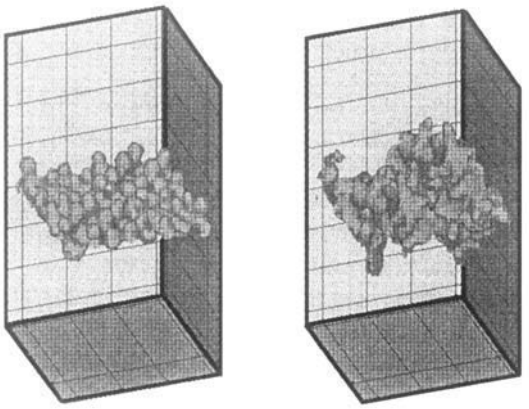

Fig. 10

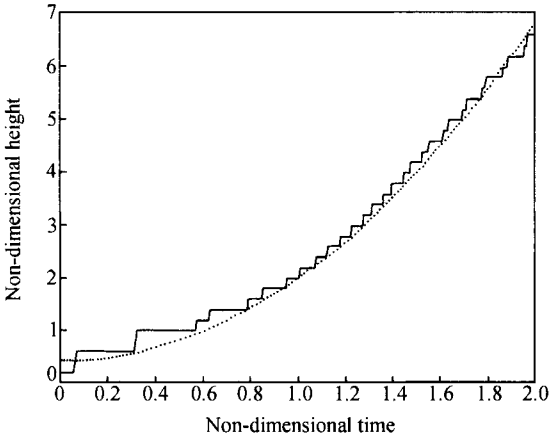

Fig. 11

As compared with other methods, the model and algorithm used in this paper show remarkable advantage in simplicity and stability. The effect of the numerical viscosity has almost been eliminated with inclusion of the molecular diffusions in both momentum and mass. With the passive scalar transport model, there is no need to track the interface in the calculation. In particular, a full treatment of the interfacial motion is addressed. It should be noted that the single-phase fluid model is valid only for the case in which the Atwood number is very low. For flow with large density ratio further improvement is expected.

Acknowledgments We thank Dr. Z.F. Zhang and Dr. Q. Zhang for their useful discussions. This work was supported by the 9th-Five-Year Climb Project of MST, the NSAF Project, the China Postdoctoral Science Foundation and CAS, and K. C. Wong Postdoctoral Research Award Fund.

References

1. Sharp, D. H., An overview of Rayleigh-Taylor instability, Physica D, 1984, 12: 3—18.
2. Baker, G. R., Meiron, D. I., Orszag, S. A., Vortex simulation of the Rayleigh-Taylor instability, Phys. Fluids, 1980, 23: 1485—1490.
3. Tryggvason, G., Numerical simulations of the Rayleigh-Taylor instability, J. Comput. Phys., 1988, 75: 253—282.
4. Mulder, W., Osher, S., Sethian, J., Computing interface motion in compressible gas dynamics, J. Comput. Phys., 1992, 100: 209—228.
5. Osher, S., Sethian, J., Fronts propagating with curvature-dependent speed: algorithms based on Hamilton-Jacobi formulations, J. Compput. Phys., 1988, 79(1): 12—49.
6. Li, X. L., Study of three-dimensional Rayleigh-Taylor instability in compressible fluids through level set method and parallel computation, Phys. Fluids, 1993, A(5): 1904—1913.
7. Holmes, R. L, Grove, J. W., Sharp, D. H., Numerical investigation of Richtmyer-Meshkov instability using front tracking,

J. Fluid Mech., 1995, 301: 51—64.

8. Gardner, C., Glimm, J., McBryan, O. et al., The dynamics of bubble growth for Rayleigh-Taylor unstable interfaces, Phys. Fluids, 1988, 31: 447—465.
9. He Xiaoyi, Chen Shiyi, Zhang Raoyang, A lattice Boltzmann scheme for incompressible multiphase flow and its application in simulation of Rayleigh-Taylor instability, J. Comput Phys., 1999, 152: 642—663.
10. Li, X. L., Jin, B. X., Glimm, J., Numerical study for the three-dimensional Rayleigh-Taylor instability through the TVD/AC scheme and parallel computation, J. Comput. Phys., 1996, 126: 343—355.
11. Taylor, G. I., The stability of liquid surface when accelerated in a direction perpendicular to their planes, I, Proc. Roy. Soc., London, 1950, A201: 192—196.
12. Abarzhi, S. I., Stable steady flow in the Rayleigh-Taylor instability, Phs. Rev. Lett., 1998, 81: 337—340.
13. Zhang, Q., The motion of single-mode Rayleigh-Taylor unstable interfaces, IMPACT Comput. Sci. Eng., 1991, 3: 277—389.
14. Deardorff. J. W., Stratocumulus-capped mixed layers derived from a three-dimensional model, Boundary Layer Meteorology, 18: 295—527.
15. Read, K. I., Experimental investigation of turbulent mixing by Rayleigh-Taylor instability, Physica D, 1984, 12: 45—58.
16. Youngs, D. L., Numerical simulation of turbulent mixing by Rayleigh-Taylor instability, Physica D, 1984, 12: 32—44.
17. Youngs, D. L., Modeling turbulent mixing by Rayleigh-Taylor instability, Physica D, 1989, 37: 270—287.
18. Moeng, G. H., A large eddy simulation model for the study of planetary boundary layer turbulence, J. Atmos. Sci., 1984, 41(13): 2052—2062.
19. Lesieur, M., Metais, Q., New trends in large-eddy simulations of turbulence, Annu. Rev. Fluid Mech., 1996, 28: 45—82.
20. Metais, Q., Lesieur, M., Spectral large-eddy simulations of isotropic and stably-stratified turbulence, J. Fluid Mech., 1992, 239: 157—194.